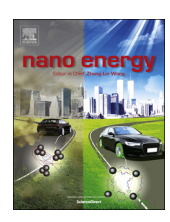


Contents lists available at ScienceDirect

Nano Energy

journal homepage: www.elsevier.com/locate/nanoen



Full paper

Catalytic mechanism and design principles for heteroatom-doped graphene catalysts in dye-sensitized solar cells



Zhenghang Zhao^a, Chun-Yu Lin^a, Jinlong Tang^{a,b}, Zhenhai Xia^{a,c,*}

- a Department of Materials Science and Engineering, Department of Chemistry, University of North Texas, Denton, TX 76203, USA
- ^b School of Science, Southwest University of Science and Technology, Mianyang 621010, China
- ^c College of Energy, Beijing University of Chemical Technology, Beijing 100029, China

ARTICLE INFO

Keywords: Dye-sensitized solar cell Carbon-based materials Catalyst design DFT calculation Heterogeneous catalysis

ABSTRACT

Doped carbon nanomaterials are promising candidates to replace expensive Pt counter electrode for catalyzing triiodide reduction reaction (IRR) in dye-sensitized solar cells (DSSCs), but trial-and-error approaches have been used to develop better catalysts. Here, design principles are developed for p-block heteroatom-doped graphene as efficient IRR catalysts through density functional theory (DFT) calculations. The descriptors based on the intrinsic properties of dopant elements are identified to establish a quantitative relationship that correlates the doped structures to catalytic activities. Moreover, a quantitative relationship is also established between the catalytic performance and the extrinsic factors such as the number of exposed active sites for a particular mass loading. It is predicted that most p-block element doped graphene catalysts have better performance than Pt, and that doping at graphene edges enhances catalytic activities. These predictions are consistent with experimental results. The proposed design principles enable us to rationally design and search for highly active catalysts based on earth-abundant, cost-effective materials.

1. Introduction

Dye-sensitized solar cells (DSSCs) have attracted much attention as a promising clean energy source owning to their potential of low cost, easy fabrication and recorded efficiency (over 10%) [1]. In a typical DSSC, there are two important reactions: the photon-induced oxidation of a dye at the TiO₂ photoanode, and the reduction of the redox species for regeneration of the dye at the counter electrode (CE) [2,3]. Iodide/ triiodide (I^-/I_3^-) are usually used as an effective redox couple for dye regeneration, but they must be catalyzed by the CE to ensure rapid reaction and low overpotential. Platinum (Pt) has been used as the standard CE in DSSCs due to its high catalytic activity for I_3^- reduction, good chemical stability, and high conductivity. However, because of the high cost and scarcity of Pt, there is the need in commercial applications for cheaper, more abundant materials for CEs in DSSCs [4]. Carbon nanomaterials are potential electrodes for DSSCs owning to their unique physical and chemical properties and abundant resources. Recently, extensive search has been made for better carbon-based catalysts for CEs, including carbon blacks [5], carbon nanoparticles [6], carbon nanotubes [7,8], graphene [9-13] and graphene oxides [14]. It has been demonstrated that heteroatom-doped carbon nanomaterials, such as oxygen-doped graphene sheets [15], 3D N-doped graphene foams [4], edge selectively antimony-doped graphene nanoplatelets [16], and N, P co-doped graphene [17], can achieve the conversion efficiency comparable to or higher than that of platinum in catalyzing triiodide reduction reaction (IRR). Although the superior catalytic capabilities of the heteroatom-doped carbon nanomaterials for the reduction of I_3^- have been demonstrated, trial-and-error approaches are still used to date for the development of highly-efficient catalysts. To rationally design a catalyst, it is necessary to establish the intrinsic relationship that correlates the doped structures to the catalytic activities of the carbon-based catalysts.

Recently, theoretical work has been performed to understand the reaction mechanism of IRR in DSSCs. Density functional theory (DFT) methods were used to analyze the binding of I_2 and I_3^- and Li $^+$ to different sites in organic sensitizers [18], the properties of the iodine/triiodide redox couple in DSSCs [19], and the rate-determining step on N-doped graphene in IRR [20]. For p-block heteroatom-doped carbon-based catalysts, however, there is a lack of design principles or an intrinsic descriptors that govern catalytic activities, which hinder the rational design of catalysts with desirable properties. To accelerate the search for highly active catalysts based on earth-abundant, cost-effective materials, it is necessary to establish design principles and strategies to predict the electrocatalytic activities of the heteroatom-doped

^{*} Corresponding author at: Department of Materials Science and Engineering, Department of Chemistry, University of North Texas, Denton, TX 76203, USA. E-mail address: zhenhai.xia@unt.edu (Z. Xia).

carbon-based catalysts in DSSCs.

In this study, for the first time, an intrinsic material property has been identified as the activity descriptor, which establishes a quantitative relationship between the descriptor and the catalytic activities of heteroatom-doped carbon-based catalysts. Such a relationship has a predictive power that enables us to design new catalysts with enhanced IRR activities. Having been verified by a number of reports for IRR activities of p-block element doped carbon nanomaterials [4,12,15-17,20-25], this descriptor provides a new base for the rational design of various new earth-abundant, cost-effective catalysts for DSSCs.

2. Computational methodology

It is commonly known that the overall reduction of the triiodide on the CE can be described as

$$I_3^- + 2e^- = 3I^- \tag{1}$$

which involves a non-electrochemical step,

$$I_3^- = I_2 + I^- \tag{2}$$

and two-electron transfer reaction

$$I_2 + 2e^- = 2I^- \tag{3}$$

The half reaction free energy of Eq. (1) is $-0.53 \, \text{eV}$ and the half reaction free energy of Eq. (3) is $-0.54 \, \text{eV}$, while the non-electrochemical step (Eq. (2)) has a reaction free energy of 0.01 eV. Since the energy needed for Eq. (2) is relatively small, the reaction can occur rapidly in equilibrium, which is a non-rate-determining step [12,26,27]. Thus our analysis will be focused on the electrochemical reaction in Eq. (3). In DSSCs, the electrochemical reaction involves several elementary steps through an associate pathway [19],

$$I_2 + * + e^- = I^- + I^* (4)$$

$$I^* + e^- = I^- + * (5)$$

where *represents the free site on a catalytic surface. This associate approach is similar to the mechanism in Heyrovsky pathway in hydrogen evolution reactions (HER) [28]. In addition, the reaction could occur through a dissociate reaction pathway,

$$I_2 + 2^* = I^* + I^* \tag{6}$$

$$I^* + I^* + e^- = I^* + I^- \tag{7}$$

$$I^* + e^- = I^- + * (8)$$

where Eq. (6) involves two active sites on a catalyst surface. This dissociate pathway is similar to the Tafel reactions in HER. The Gibb's free energies for the sub-reactions are calculated by

$$\Delta G = \Delta E + \Delta Z P E - T \Delta S + \Delta G_U \tag{9}$$

where ΔE and $T\Delta S$ are the reaction free energy and the entropy influence of each step, respectively, which are obtained from DFT calculations, ΔZPE is the change in zero-point energies that is obtained from the vibrational frequencies of adsorbed intermediates (I^* , I_3^- and I^-) without the solvent corrections using the density functional perturbation theory (DFPT), and ΔG_U is the potential applied at electrodes. After the calculations of Gibb's free energies for the reactions, the overpotentials $\eta^{\rm IRR}$ of the electrochemical reactions in DSSCs can be determined by:

$$\eta^{IRR} = Max(\frac{\Delta G_4}{e} + 0.54 \quad or \frac{\Delta G_5}{e} + 0.54)$$
(10)

in which ΔG_4 and ΔG_5 are the Gibb's free energies of Eqs. (4) and (5). Since the equilibrium potential for a half reaction of IRR is -0.54 eV, the overpotential η is the extra energy needed for the reaction than thermodynamically expected [29]. An ideal catalyst should be able to facilitate IRR just above the equilibrium potential (U^0), with zero

overpotential ($\eta=0$). However, the ideal case cannot be achieved in general because the binding energies of the intermediates are correlated [30]. Therefore, thermodynamically, a catalyst with lower η would have better catalytic performance.

DFT calculations were performed to predict the catalytic activities of the p-block-element-doped graphene as catalytic CEs in DSSCs. Vienna Ab-initio Simulation Package (VASP) was used to perform the DFT simulations. Projector augmented wave (PAW) pseudopotential was used to describe the correlation between the pseudo-core and outer shell electrons. Specifically, C-2s22p2, O-2s22p4, H-1s1 were treated as valence electrons. The generalized gradient approximation (GGA) developed by Perdew, Burke and Ernzerhof (PBE) was utilized as the electronic exchange and interaction principles. A 480 eV cut off energy of the plane wave basis was set to maintain the accuracy of the calculations. 10^{-5} eV was the convergence limitation for the electron relaxing and 10^{-2} eV was for the ion relaxing. Non-spin polarized set was used throughout the whole study.

Three categories of graphene unit cells were built to perform the calculations, and Pt (111) unit cell was also constructed for comparison. The first one is a graphene nanoribbon containing 4×5 hexagonal rings with zigzag edges. The dimensions of the unit box are $9.85\,\text{Å} \times 24.00\,\text{Å} \times 18.00\,\text{Å}$ with a periodic boundary condition along a direction, leaving enough spaces along b and c directions so that the reactions can be studied accordingly. In the simulation, K-point mesh is set to be $4 \times 1 \times 1$. A heteroatom was doped on the edges and in the middle of the graphene (Supplementary Fig. S1A). The second one is a graphene nanoribbon with armchair edge. Its size is $8.60\,\text{Å} \times 24.00$ $\rm \mathring{A} \times 18.00\,\mathring{A}$ with similar boundary conditions as the last one and Kpoint meshing is $4 \times 1 \times 1$ (Supplementary Fig. S1B) with heteroatom doped on the edge and in the middle of the graphene as well. The third one is an edgeless graphene with 4 × 7 hexagonal rings giving a $17.04 \,\text{Å} \times 9.84 \,\text{Å} \times 18.00 \,\text{Å}$ unit box and a heteroatom was doped at the center of the graphene surface (Supplementary Fig. S1C). Various types of heteroatoms were studied as the dopants including B, N, P, Si, O, S, Se, F, Cl and Br. For comparison, a unit cell for Pt with (111) free surface were also built (Supplementary Fig. S1D) with a volume of $10.55 \,\text{Å} \times 9.30 \,\text{Å} \times 25.00 \,\text{Å}$ containing five layers of Pt atoms. The Kpoint meshing for the metallic models is $4 \times 4 \times 1$. Besides, three special structures were also considered, which are Chalcogen (O, S, Se)doped graphene (Supplementary Fig. S1E), Halogen (F, Cl, Br)-doped graphene (Supplementary Fig. S1F), S-O2 and P-O2 armchair/zigzag graphene (Supplementary Fig. S1G, S1H). As all these models have many identical active sites, a notation mechanism was developed to clearly describe the positions of the active sites on the catalytic surface (Supplementary Fig. S2, S3). The solvent is assumed to be acetonitrile. To confirm the Pt model used in this study, the calculations of oxygen reduction reaction (ORR) were performed on this model by using the overpotential approach. The overpotential of ORR on the Pt was 0.48 V comparing to 0.45 V from Nørskov's work [29]. We also confirm the Pt model for HER. The overpotential of HER calculated from our model is 0.12 V, which is comparable to 0.09 V from Nørskov's work [31], indicating our platinum model is reasonably good.

3. Results and disscussions

3.1. Gibb's energy and overpotentials of IRR

To rationally search for the best carbon-based catalyst, free energies and overpotentials for elementary reactions of IRR (Eqs. (4)–(8)) were calculated for all the possible active sites on graphene structures doped with p-block elements, X (X = N, B, P, S, Si, Se, F, Cl, Br, I, P-OH, S-OH, P-O₂, Se-O₂ and S-O₂, etc.) (Fig. 1A, Supplementary Fig. S1), and determined the rate-limiting step by selecting the maximum overpotentials in the elementary reaction steps. The doping positions on each structure were changed with respect to the graphene edge to reveal the edge effect of doping sites (Supplementary Fig. S2). For

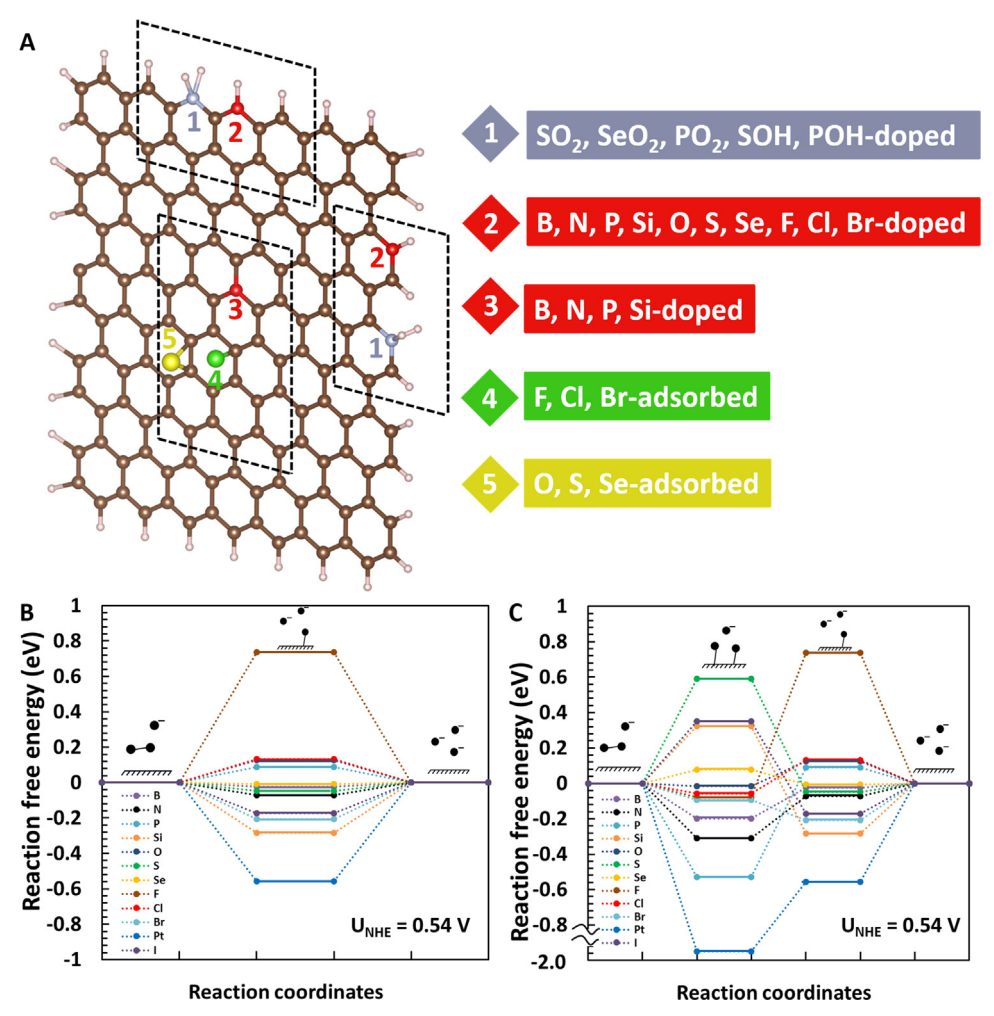


Fig. 1. The atomic models and free energy diagrams for X-doped graphene sheets and nanoribbons. (A) Schematic figure of the X-doped graphene nanoribbon models with various edge conditions and dopants. Free energy diagram of X-doped graphene and Pt (111) surface with (B) associate pathway and (C) dissociate pathway at an electrode potential of 0.54 V.

comparison, edgeless graphene and transition metal Pt with (111) surface were also built (Supplementary Fig. S2D and S3). Supplementary Fig. S4 shows a typical IRR processes occurring on the surface of N-doped graphene for both dissociate and associate pathways. In dissociate pathway, since IRR occurred with two I atoms adsorbed on different positions at the same time, each model was calculated by introducing various combinations of adsorptions at different active sites (Supplementary Fig. S5).

The overpotentials for doped graphene and Pt were calculated and the best doped structure for each dopant element was identified (Supplementary Table S1). Figs. 1B and 1C show the free energy diagrams of IRR for the best doped structures under an equilibrium potential of 0.54 V. The free energy diagrams of 0 V potential of both associate and dissociate pathways are shown in Supplementary Fig. S6. In general, the overpotential of X-doped graphene is much lower than that of benchmark Pt, depending on the type of dopants. Our calculations demonstrate that dissociate pathway is not favorable for S, Se, Si, Cl and I-doped graphene due to their high dissociation energies of I₂ onto two sites. Previous work showed that compared with the dissociate reaction pathway, the associate pathway seems more energetically favorable in terms of low interaction for N-doped graphene [20]. Se and B-doped graphene nanoribbons show the lowest and second lowest overpotentials (8 mV, 24 mV), respectively, which are much lower than Pt (0.56 V). Chalcogen-element (e.g., O, and S), P and N-doped graphene nanoribbons also yield low overpotentials comparable to Pt, while halogen element-doped graphene shows relatively higher

overpotential than that of chalcogen-doped one, but still lower than that of the Pt except for fluorine. These predictions are supported by the experimental results, for example, Se-doped graphene showed much better electrochemical properties than Pt [12], and N-doped carbon nanomaterials yielded higher short circuit current than Pt [4].

3.2. Intrinsic descriptors that govern the catalytic activities

To search for the best catalysts, it is necessary to establish a design rule or descriptor that relates material parameters to catalytic activities. In the first step, the adsorption energies of reaction species on the catalysts were used as a descriptor, and the lowest IRR overpotential for each dopant was plotted against the adsorption energy of I* for X-doped graphene nanoribbons, yielding a volcano plot with B and Se at the summit, as shown in Fig. 2A. Volcano plots of all calculated data can be found in Supplementary Fig. S7. The adsorption energy of I* is calculated by,

$$\Delta G_{I^*} = G(graphene + I^*) - G(graphene) - \frac{1}{2}G(I^2)$$
(10)

Thus, the adsorption energy of I* can be used as an effective descriptor to describe catalytic activities. Overall, most of the X-doped graphene nanoribbons have relatively lower adsorption energy compared with the adsorption energy of Pt ($-0.56\,V$). The best catalyst should locate at the summit of the volcano, at which both the overpotential and the adsorption energy are equal to zero. B, N, O, S and Se-

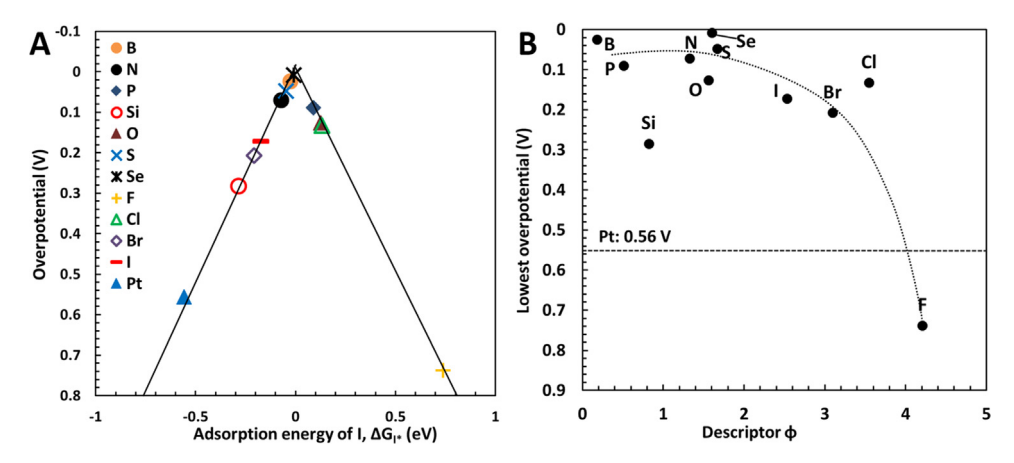


Fig. 2. Predicted and calculated volcano plots of X-doped graphene. (A) Calculated overpotential vs. the adsorption energy of I* on heteroatom-doped graphene; (B) The lowest overpotential of each doped-graphene as a function of descriptor φ.

doped graphene sheets are located close to the peak, indicating high catalytic activities. Among the p-block elements, F-doping results in a highly positive adsorption energy probably due to its highest electronegativity. According to Sabatier principle, the interaction between the catalysts and the adsorbates should be neither too strong nor too weak. For fluorine-doped graphene, the interaction between the fluorine and adsorbates is probably too strong because of electronegative enrichment of electron density to F side, consequently leading to the low catalytic activities. Interestingly, while the electronegativity of halogen family from Cl, Br, to I gradually reduces, their catalytic activities increase compared with F, as demonstrated experimentally [43].

Although the adsorption energy of I* is a good descriptor for the doped graphene, it is not intrinsic material property, and it is inconvenient in determining relationship between material structures and catalytic activities. To predict the electrocatalytic properties of the doped carbon nanomaterials for IRR in DSSCs, we introduced a descriptor that was previously identified for ORR and oxygen evolution reaction (OER) [32,33]. This descriptor ϕ can be written as,

$$\phi = \frac{E_X A_X}{E_C A_C} \tag{11}$$

where E_X and E_C are electronegativities of the dopant and carbon, A_X and A_C are electron affinities of the dopant and carbon. The overpotentials on the most active sites of each X-doped graphene nanoribbon were plotted as a function of the descriptor (Fig. 2B). This descriptor leads to a fitting curve that correlates the doped structures to the catalytic activity of the carbon-based catalysts, from which the best dopant can be predicted. As shown in Fig. 2B, for dopants, the lower the descriptor ϕ , the better the doped graphene catalysts perform. With the help of this descriptor, one can predict heteroatom-doped graphene catalysts with desirable catalytic property for DSSCs.

3.3. Edge effect of the doped graphene

Graphene contains different edges (e.g., armchair and zigzag edges) that can be tuned to enhance specific properties. This edge effect has been demonstrated to affect the catalytic activity for various catalytic process, such as OER, ORR and HER [32–40]. We have calculated the overpotentials of non-edged and edged graphene with different doping positions. The overpotential is plotted as a function of the distance between N, B, P dopants and the edges (Fig. 3A). With increasing the distance from the dopant to the edge, the overpotential decreases and achieves a minimum at 2.153 Å for N- and P-doped graphene, but the minimum overpotential of B-doped graphene is at 3.920 Å. These results imply that it would be more efficient to dope the elements (e.g., P and N) near the graphene edges and the best range is between 2 Å and 4 Å from the edge. On the other hand, the overpotential is also

correlated with the distance between active sites and the edge for a dopant located at the edge (Fig. 3B). For B-doped graphene, the minimum overpotential occurs when the distance between the active site and the edge is small, while for N-doped and P-doped graphene, the minimum overpotentials occur when the distance between the active site and the edge is large. In other words, introduction of more graphene edges would significantly enhance the catalytic activities. Therefore, the IRR performance of the heteroatom-doped graphene would be promoted by taking advantage of the edge effect of the graphene nanosheets.

The good performance of doped graphene for IRR is attributed to the electron transfer between the dopants and surrounding carbon atoms. After doping, the electron transfer from carbon atoms to the dopants, resulting in positively charged positions on the graphene surface (Supplementary Fig. S8). Charge transfer was thus calculated by Bader charge analysis [41]. Figs. 3C to 3F shows the charge transfer and the most active sites of N-doped with zigzag edge, S-doped with armchair edge, F-doped with zigzag edge and N-doped non-edge graphene. Those active sites carrying large positive charges are potentially ones for the IRR on graphene while those with large negative charges are not good catalysts for IRR such as F-doped graphene, as shown in Fig. 3E. Similar results are reported for other electrocatalytic reactions such as OER and ORR, which concluded the essence of the positive charge on the catalytic surface [32,33,37]. Therefore the heteroatomdoping leads to electron transfer on the graphene surface, and thus enhance the electrochemical properties of the materials for IRR.

3.4. Catalyst design principles

As discussed above, the type of dopants and edges are two main factors that determine the catalytic activities of heteroatom-doped graphene. Thus, the first design principle developed in this work is the descriptor that can be used to select the best dopant for the carbon-based catalysts for IRR in DSSCs. As expected, in addition to particular physicochemical properties, the value of adsorption energy, ΔG_{I*} controls the performance of a catalyst. The second strategy is introduction of more edges in the carbon-based catalysts, which further enhance the electrochemical performance of the catalysts. The above strategies exploit the intrinsic properties of the materials (dopants and doping structures) to enhance the catalytic performance.

In addition to the unit activity on each active site (intrinsic), a catalyst is also governed by the number of exposed active sites for a particular mass loading (extrinsic). Thus, we propose the third design strategy by establishing the relationship between the apparent activities of graphene-based materials with corresponding number of active sites. The activities or the overall current density under different electrode potentials are computed via the classic Butler-Volmer relation based on

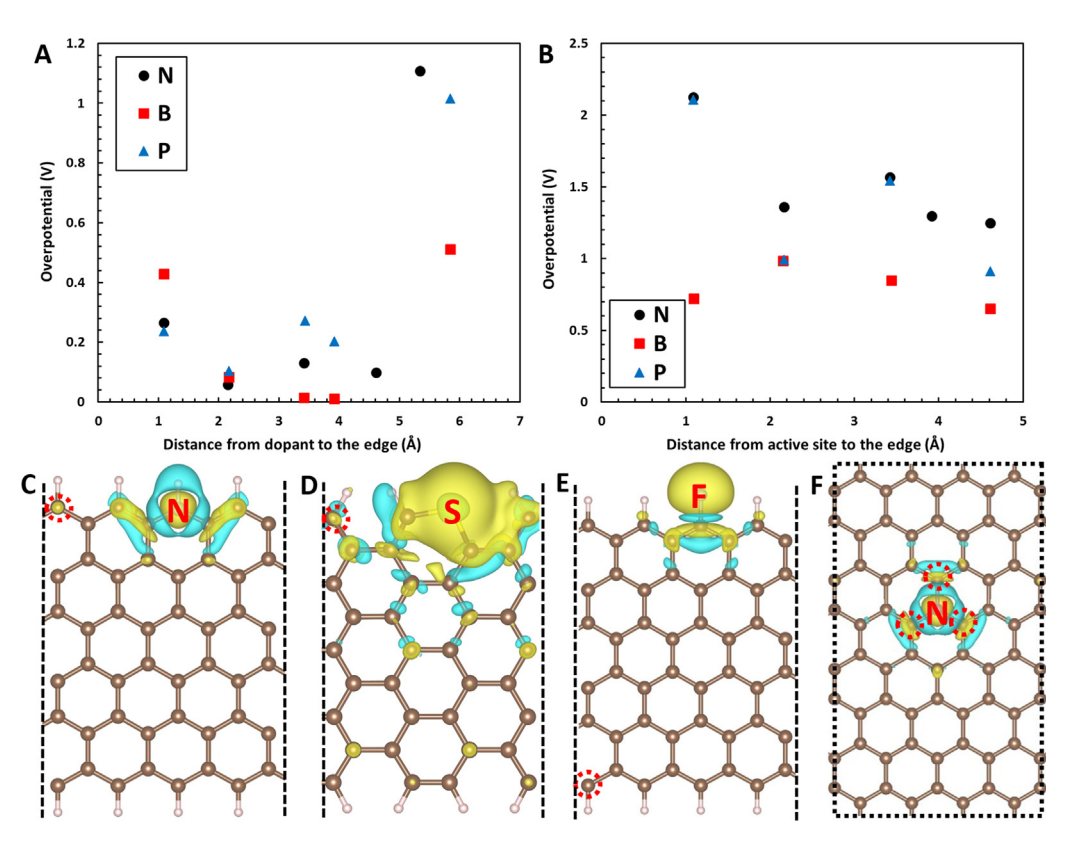


Fig. 3. Edge effect and charge transfer of heteroatom-doped graphene. (A) Overpotential of the active sites at the edge as a function of the distance from dopant to the edge, and (B) Overpotential as a function of the distance from an active site to the edge for a dopant fixed at the graphene edge. Charge transfer analysis of (C) N-doped zigzag graphene, (D) S-doped armchair graphene, (E) F-doped zigzag graphene and (F) N-doped non-edged graphene. The isosurface level is 0.003. Color legend: Brown balls are carbon; white balls are hydrogen. Blue color indicates positive charge and yellow color indicates negative charge.

the ideal current for a predicted X-doped graphene sample. Four physicochemical properties of graphene were considered: the surface area, heteroatom doping levels, loading mass and test area. According to the Butler-Volmer Equation, given the exchange current for an active site is i_0 /site, the electrode current per site i under electrode potential U is 28

$$i(U) = -i_0 \cdot e^{-\frac{U - U_0}{b}} \tag{12}$$

where U_0 is the relative potential, and b is the Tafel slope. The current density (in mA.cm⁻²), j, of an electrode under U is then computed from

$$j(U) = i(U) \cdot \frac{S \cdot m}{S_c} \cdot \frac{\zeta}{A} \tag{13}$$

where S is the surface area per mass loading (in $m^2\ g^{-1}$), m is the loading amount of catalyst material (g), S_c is the area per carbon atom (in $1.677\times 10^{-18}\ m^2$) and ζ is the doping percentage of active heteroatoms. Thus, if the site current is the same (i.e., the same dopant), the electrode current density should be proportional to the number of active sites on the catalyst surface.

The extrinsic design principle is verified by the experimental results on nitrogen-doped graphene for the IRR catalytic activity. In DSSCs, current density is considered to well represent the IRR catalytic activities of electrocatalysts. We carefully selected the experimental data reported for N-doped graphene and pristine graphene with dopant content, BET surface area and test area mentioned, and made plots of the short circuit current as a function of the number of active sites (Supplementary Table S2, Fig. 4A) [4,22,42]. To reliably compare the data from different sources, the current density is normalized by the benchmarked Pt CE current density measured under the same condition in the same experiment. The normalized current density linearly increases with increasing the number of active sites available for IRR, which is consistent with theoretical predictions (Eq. (13)).

The descriptor φ was also verified by the experimental results on heteroatom-doped graphene for the IRR catalytic activity [4,12,22,42–45]. Since the current density cited in the literatures was

measured under different conditions, and BET surface area and content of the dopants are different from each other, we carefully selected the experimental data reported for p-element-doped graphene (Supplementary Table S3). The current density is firstly normalized by the benchmarked Pt CE current density measured under the same condition in the same experiment, and then normalized by the current density of N-doped graphene at the same active site. The normalized current density versus the descriptor ϕ is plotted in Fig. 4C. The IRR activity of doped carbon nanomaterials is higher than that of Pt when the value of ϕ is smaller than 3. This relationship is consistent with the predictions from our calculations, as shown in Fig. 2B. Thus, the experimental data support that the primary descriptor governs the IRR activity of the p-element-doped carbon nanomaterials, as demonstrated theoretically in this work.

4. Conclusions

In conclusion, triiodide reduction reactions on heteroatom-doped graphene in DSSCs was studied via density functional theory method. The results showed that p-element-doped graphene have relatively low overpotential than that of Pt (111), and their catalytic performance could be better than Pt for triiodide reduction in DSSCs. A descriptor related to electronegativity and electron affinity was identified to be able to establish a quantitative relationship that correlates the doped structures to the catalytic activity, from which the best dopant can be rationally designed and synthesized. Heteroatom-doping results in positive charge on some carbon atoms near a dopant, which enhances the electrochemical reactions of triiodide reduction. Introducing more edges in doped graphene or dope the dopant near the edge could improve the electrochemical performance. In addition, an extrinsic design principle is proposed and verified by the experimental results on nitrogen-doped graphene for the IRR catalytic activity. This work provides a theoretical base for better understanding of triiodide reduction occurring in DSSCs and design rules for metal-free carbon nanomaterial based catalyst for DSSCs.

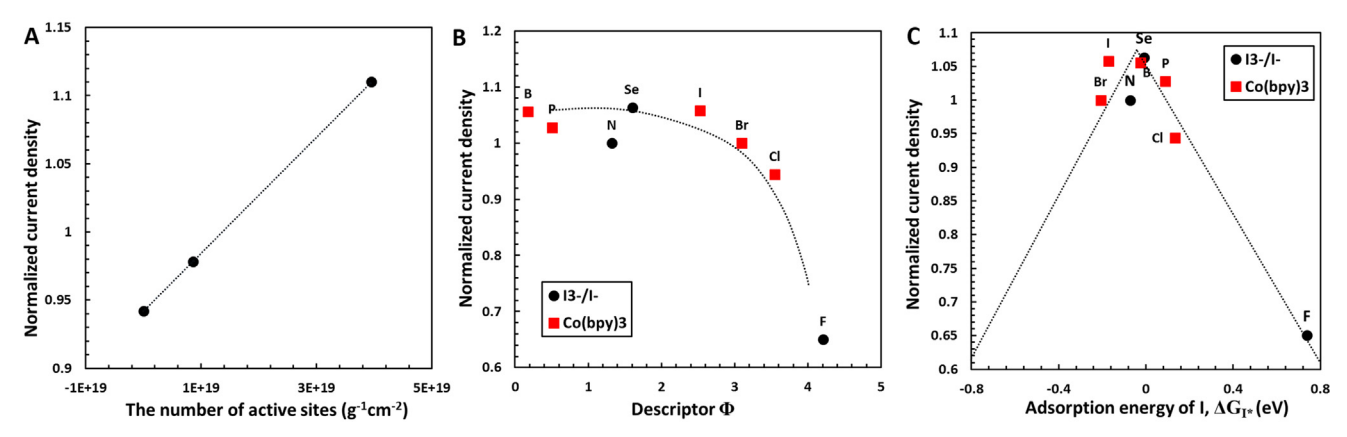


Fig. 4. The experimental results for normalized current density as a function of the descriptors. (A) Average current density for N-doped graphene electrode, normalized by the benchmarked Pt CE current density measured under the same condition in the same experiment for IRR, as a function of the number of active sites (product of BET surface area and percentage of dopant content and divided by test area) [4,22,42,46], (B) Measured current density, normalized by the current density for N-doped graphene with the same number of active sites, as a function of the descriptor Φ of dopants [4,12,22,42-45], and (C) Normalized current density as a function of the adsorption energy of I, ΔG_{I*} on the graphene surface.

Acknowledgements

We thank the National Key Research and Development Program of China (2017YFA0206500), and National Science Foundation (1561886, 1363123 and 1662288) and Air Forces MURI program (#FA9550-12-1-0037) for the support of this research. Computational resources were provided by UNT high performance computing initiative, a project of academic computing and user services within the UNT computing and information technology center.

Appendix A. Supporting information

Supplementary data associated with this article can be found in the online version at http://dx.doi.org/10.1016/j.nanoen.2018.04.053.

References

- [1] Y. Chiba, A. Islam, Y. Watanabe, R. Komiya, N. Koide, L. Han, Jpn. J. Appl. Phys. Part 2 Lett. 45 (2006) 638.
- M. Grätzel, J. Photochem. Photobiol. C Photochem. Rev. 4 (2003) 145.
- [3] B. O'Regan, M. Gratzel, Nature 353 (1991) 737.
- Y. Xue, J. Liu, H. Chen, R. Wang, D. Li, J. Qu, L. Dai, Angew. Chemie Int. Ed. 51 (2012), p. 12124.
- T.N. Murakami, S. Ito, Q. Wang, M.K. Nazeeruddin, T. Bessho, I. Cesar, P. Liska, R. Humphry-Baker, P. Comte, P. Péchy, M. Grätzel, J. Electrochem. Soc. 153 (2006)
- [6] R. Jia, J. Chen, J. Zhao, J. Zheng, C. Song, L. Li, Z. Zhu, J. Mater. Chem. 20 (2010) 10829.
- E. Ramasamy, W.J. Lee, D.Y. Lee, J.S. Song, Electrochem. Commun. 10 (2008)
- [8] G. Yue, J. Zhang, J. Liu, X. Lu, Z. Hu, Y. Zhu, J. Mater. Sci. Mater. Electron. 27 (2016) 4736.
- Z. Yang, T. Chen, R. He, G. Guan, H. Li, L. Qiu, H. Peng, Adv. Mater. 23 (2011)
- [10] J. Han, H. Kim, D.Y. Kim, S.M. Jo, S.-.Y. Jang, 2010.
- [11] X. Wang, L. Zhi, K. Müllen, Nano Lett. 8 (2008) 323.
- M.J. Ju. I. Jeon, H.M. Kim, J. Il Choi, S. Jung, J. Seo, I.T. Choi, S.H. Kang, H.S. Kim, M.J. Noh, J. Lee, H.Y. Jeong, H.K. Kim, Y. Kim, J. Baek, Sci. Adv. (2016) 1.
- [13] W.-T. Wu, S.-H. Yang, C.-M. Hsu, W.-T. Wu, Diam. Relat. Mater. 65 (2016) 91.
- [14] M. Yu, J. Zhang, S. Li, Y. Meng, J. Liu, J. Power Sources 308 (2016) 44.
- [15] J.D. Roy-mayhew, D.J. Bozym, C. Punckt, I. a. Aksay, ACS Nano 4 (2010) 6203. H.M. Kim, I.-Y. Jeon, I.T. Choi, S.H. Kang, S.-H. Shin, H.Y. Jeong, M.J. Ju, J.-[16] B. Baek, H.K. Kim, J. Mater. Chem. A 4 (2016) 9029.
- M. Chen, L.-L. Shao, Y.-X. Guo, X.-Q. Cao, Chem. Eng. J. 304 (2016) 303. [17]
- [18] M. Pastore, E. Mosconi, F. De Angelis, J. Phys. Chem. C 116 (2012) 5965.
- [19] G. Boschloo, A. Hagfeldt, Acc. Chem. Res. 42 (2009) 1819.
- Y. Zhang, J. Hao, J. Li, C. Hao, Theor. Chem. Acc. 135 (2016) 23. [20]
- [21] Z. Wang, P. Li, Y. Chen, J. He, J. Liu, W. Zhang, Y. Li, J. Power Sources 263 (2014) 246
- [22] G. Wang, W. Xing, S. Zhuo, Electrochim. Acta 92 (2013) 269.
- M.J. Ju, J.C. Kim, H.J. Choi, I.T. Choi, S.G. Kim, K. Lim, J. Ko, J.J. Lee, I.Y. Jeon, J.B. Baek, H.K. Kim, ACS Nano 7 (2013) 5243.
- S. Hou, X. Cai, H. Wu, X. Yu, M. Peng, K. Yan, D. Zou, Energy Environ. Sci. 6 (2013)

3356.

- [25] H.Q. Fang, C. Yu, T.L. Ma, J.S. Qiu, Chem. Commun. 50 (2014) 3328.
- [26] Y. Hou, D. Wang, X.H. Yang, W.Q. Fang, B. Zhang, H.F. Wang, G.Z. Lu, P. Hu, H.J. Zhao, H.G. Yang, Nat. Commun. 4 (2013) 1583.
- a. Hauch, a. Georg, Electrochim. Acta 46 (2001) 3457.
- [28] N.M. Marković, B.N. Grgur, P.N. Ross, J. Phys. Chem. B 101 (1997) 5405.
- [29] J.K. Nørskov, J. Rossmeisl, a. Logadottir, L. Lindqvist, J.R. Kitchin, T. Bligaard, H. Jónsson, J. Phys. Chem. B 108 (2004) 17886.
- [30] I.C. Man, H.Y. Su, F. Calle-Vallejo, H. a. Hansen, J.I. Martínez, N.G. Inoglu, J. Kitchin, T.F. Jaramillo, J.K. Nørskov, J. Rossmeisl, ChemCatChem 3 (2011) 1159.
- [31] J.K. Nørskov, T. Bligaard, a. Logadottir, J.R. Kitchin, J.G. Chen, S. Pandelov, U. Stimming, J. Electrochem, Soc. 152 (2005) J23.
- Z. Zhao, Z. Xia, ACS Catal. (2016) 1553.
- [33] Z. Zhao, M. Li, L. Zhang, L. Dai, Z. Xia, Adv. Mater. 27 (2015) 6834.
- [34] M. Li, L. Zhang, Q. Xu, J. Niu, Z. Xia, J. Catal. 314 (2014) 66.
- [35] L. Zhang, J. Niu, L. Dai, Z. Xia, Langmuir 28 (2012) 7542.
- [36] L. Zhang, J. Niu, M. Li, Z. Xia, J. Phys. Chem. C 118 (2014) 3545.
- [37] L. Zhang, Z. Xia, J. Phys. Chem. C 115 (2011) 11170.
- [38] Z. Zhao, L. Zhang, Z. Xia, J. Phys. Chem. C 120 (4) (2016) 2166-2175. [39] Z. Zhao, Z. Xia, MRS Adv. (2016) 1.
- [40] J. Zhang, Z. Zhao, Z. Xia, L. Dai, Nat. Nanotechnol. 10 (2015) 444.
- [41] G. Henkelman, A. Arnaldsson, H. Jónsson, Comput. Mater. Sci. 36 (2006) 354.
- [42] I.-Y. Jeon, H.-J. Choi, M.J. Ju, I.T. Choi, K. Lim, J. Ko, H.K. Kim, J.C. Kim, J.-J. Lee, D. Shin, S.-M. Jung, J.-M. Seo, M.-J. Kim, N. Park, L. Dai, J.-B. Baek, Sci. Rep. 3 (2013) 2260.
- [43] I.Y. Jeon, H.M. Kim, I.T. Choi, K. Lim, J. Ko, J.C. Kim, H.J. Choi, M.J. Ju, J.J. Lee, H.K. Kim, J.B. Baek, Nano Energy 13 (2015) 336.
- S.M. Jung, I.T. Choi, K. Lim, J. Ko, J.C. Kim, J.J. Lee, M.J. Ju, H.K. Kim, J.B. Baek, Chem. Mater. 26 (2014) 3586.
- S. Das, P. Sudhagar, V. Verma, D. Song, E. Ito, S.Y. Lee, Y.S. Kang, W. Choi, Adv. Funct. Mater. 21 (2011) 3729.
- L. Kavan, J.H. Yum, M. Grätzel, ACS Nano 5 (2011) 165.



Zhenghang Zhao received his Ph.D. in 2017 from the department of Materials Science and Engineering at the University of North Texas. He was working as a research assistant in Prof. Zhenhai Xia's group. His research interests are using multilevel computations to understand the heterogeneous catalysis and develop design guidelines to understand the electrochemical properties of novel materials. His research involves high-performance computing, materials informatics and quantum chemistry.



Chun-Yu Lin is a PhD candidate in the group of Prof. Zhenhai Xia and in Department of Materials Science and Engineering at the University of North Texas. His current scientific interests are focus on carbon nanomaterials, heterogeneous catalysis, and design principle in catalysts, energy conversion and storage materials which are related to fuel cell, metal-air batteries, solar cells and water-splitting.



Zhenhai Xia is a professor of Department of Materials Science and Engineering, and Department of Chemistry at University of North Texas, USA. His current research interests include multiscale and multi-physics modeling (finite element analysis, molecular dynamics, and DFT, etc.); materials for clean energy conversion and storage (fuel cell metal-air batteries and water-splitting, supercapacitors, solar cells, etc.), biological and bioinspired materials (e.g., than the supercapacitors, solar cells, etc.), biological and bioinspired materials (e.g., the lading, micromanipulation and assembly), and mechanics of materials (nanocomposites, high-entropy alloys).



Jinlong Tang joined Southwest University of Science and Technology in 2008 and is now an Associate Professor at the School of Science. He received his B.S. (2001) and M.S. (2004) in physics from Sichuan Normal University, and Ph.D. (2008) in Material physics and chemistry from the University of Electronic Science and Technology of China, Chengdu, China. From 2016–2017, he was as a visiting scholar in Prof. Zhenhai Xia's group at the University of North Texas. His research interests include preparation and applications of metal-semiconductor hybrid devices and the theory and computational simulation of low dimensional nano-materials.